Phonon-assisted proton tunneling in the hydrogen-bonded dimeric selenates of Cs3H(Se04)2

The Journal of Chemical Physics

Phonon-assisted proton tunneling in the hydrogen-bonded dimeric selenates of $Cs_3H(SeO_4)_2$

Cite as: J. Chem. Phys. **152**, 154502 (2020); https://doi.org/10.1063/1.5145108
Submitted: 14 January 2020 . Accepted: 25 March 2020 . Published Online: 16 April 2020

Hiroshi Matsui, Kazuki Shimatani, Yuka Ikemoto, Takahiko Sasaki, and Yasumitsu Matsuo

The Journal of Chemical Physics ARTICLE scitation.org/journal/jcp

Phonon-assisted proton tunneling in the hydrogen-bonded dimeric selenates of $Cs_3H(SeO_4)_2$

Cite as: J. Chem. Phys. 152, 154502 (2020); doi: 10.1063/1.5145108
Submitted: 14 January 2020 • Accepted: 25 March 2020 •
Published Online: 16 April 2020

Hiroshi Matsui,[1,a] Kazuki Shimatani,[1] Yuka Ikemoto,[2] Takahiko Sasaki,[3] and Yasumitsu Matsuo[4]

AFFILIATIONS

[1] Department of Physics, Graduate School of Science, Tohoku University, Sendai 980-8578, Japan
[2] SPring-8, Japan Synchrotron Radiation Research Institute, Sayo, Hyogo 679-5198, Japan
[3] Institute for Materials Research, Tohoku University, Sendai 980-8577, Japan
[4] Department of Life Science, Faculty of Science & Engineering, Setsunan University, Neyagawa 572-8508, Japan

[a] **Author to whom correspondence should be addressed:** hiroshi.matsui.b2@tohoku.ac.jp

ABSTRACT

In phases III and IV of $Cs_3H(SeO_4)_2$, the vibrational state and intrabond transfer of the proton in the dimeric selenates are systematically studied with a wide range of absorbance spectra, a spin–lattice relaxation rate of ^{1}H-NMR (T_1^{-1}), and DFT calculations. The OH stretching vibrations have extremely broad absorption at around 2350 (B band) and 3050 cm^{-1} (A band), which originate from the 0–1 and 0–2 transitions in the asymmetric double minimum potential, respectively. The anharmonic-coupling calculation makes clear that the A band couples not only to the libration but also to the OH bending band. The vibrational state (nano-second order) is observed as the response of the proton basically localized in either of the two equivalent sites. The intrabond transfer between those sites (pico-second order) yields the protonic fluctuation reflected in T_1^{-1}. Together with the anomalous absorption [ν_{p2} phonon, libration, tetrahedral deformation (δ_{440}), and 610-cm^{-1} band], we have demonstrated that the intrabond transfer above 70 K is dominated by the thermal hopping that is collectively excited at 610 cm^{-1} and the phonon-assisted proton tunneling (PAPT) relevant to the tetrahedral deformation [PAPT(def)]. Below 70 K, T_1^{-1} is largely enhanced toward the antiferroelectric ordering and the distinct splitting emerges in the libration, which dynamically modulates the O(2)–O′(2) distance of the dimer. The PAPT(lib) associated with the libration is confirmed to be a driving force of the AF ordering.

I. INTRODUCTION

Proton transfer is an important functionality in hydrogen-bonded systems such as fuel-cell electrolytes,[1,2] biological materials,[3] and novel protonic devices.[4] There are numerous types of hydrogen-bonded systems with and without water molecules.[5,6] For instance, protons in Nafion and the corresponding polymer electrolytes transfer via a plenty of randomly distributed water molecules.[7] Hydrophobic carbon nanotubes contain a regulated water network, the structure of which depends on the chirality.[8] Hydrophilic nanochannels in molecular porous crystals also accommodate a regulated water network such as a water chain or water nanotube.[9–12] Furthermore, water networks in proteins and polysaccharides such as collagen and chitosan have a bioprotonic functionality such as fuel cells,[13] field effect transistors,[14,15] and biosensors.[16–18] To create a next generation of fuel cells, high proton conductivity at room temperature is desired in a solid electrolyte without water molecules.[19–21] In such electrolytes, the proton transport occurs via the crystal lattice so that the conducting mechanism must be dependent on proton–lattice (PL) or proton–phonon interactions. Several theoretical calculations on PL interactions were done in proton conductors,[22–24] whereas little knowledge has been obtained experimentally.

Many experiments have been carried out in superprotonic conductors consisting of a tetrahedral ion MO_4^{2-} (M = S, Se, and P).[25–31] Among them, $Cs_3H(SeO_4)_2$ is a typical system that undergoes the

superprotonic conducting state (paraelastic state, phase I) with trigonal symmetry above $T_{I\text{-}II}$ = 456 K.[32–37] In the monoclinic phase (ferroelastic state) below $T_{I\text{-}II}$, the proton is basically localized in the dimer [$(SeO_4H)SeO_4$], where two SeO_4 tetrahedra are connected by a O–H···O hydrogen bond.[38] Further phase transitions take place at $T_{II\text{-}III}$ = 369 K and $T_{III\text{-}IV}$ = 50 K.

In phases III and IV, the O(2)–O′(2) segment with the distance of 2.54 Å is parallel to the *a* axis in Fig. 1(a), where the proton is shown by blue circles. In Fig. 1(b), the dimer layer and Cs one are alternately stacked along the *c* direction. Lengths and angles of the selenate and dimer are denoted in Figs. 1(c) and 1(d), respectively.[39] In phase II, however, the segment tilts to about 30° against the *b* axis on the *ab* plane. The proton basically trapped inside of O(2)–O′(2) holds the two equivalent sites. From the neutron diffraction experiment at 300 K, the separation between them is determined to be 0.52 Å.[40] The protonic motion in those sites, which is referred to as an intrabond transfer,[24] is expected to occur even in the localized phases. The quantum-statistical calculations for $M_3H(XO_4)_2$ families suggest that the interbond transfer together with the intrabond one yields the superprotonic conduction of phase I.[41–43] Moreover, a proton transfer in hydrogen-bonded systems has been theoretically studied in terms of a phonon-assisted proton tunneling (PAPT),[44–46] where the protonic potential is dynamically varied through a lattice modulation due to a corresponding phonon. A PL interaction is essential to generating a PAPT, which probably brings different temperature dependences from a conventional proton tunneling, as observed in LDS-1 with a rigid double minimum potential.[47] Particularly in superprotonic conductors, PAPT may be a fundamental mechanism of intrabond and interbond transfers. To deeply understand the transfer mechanism of $Cs_3H(SeO_4)_2$, we need to observe a protonic excitation and to make clear which phonon contributes to the PAPT.

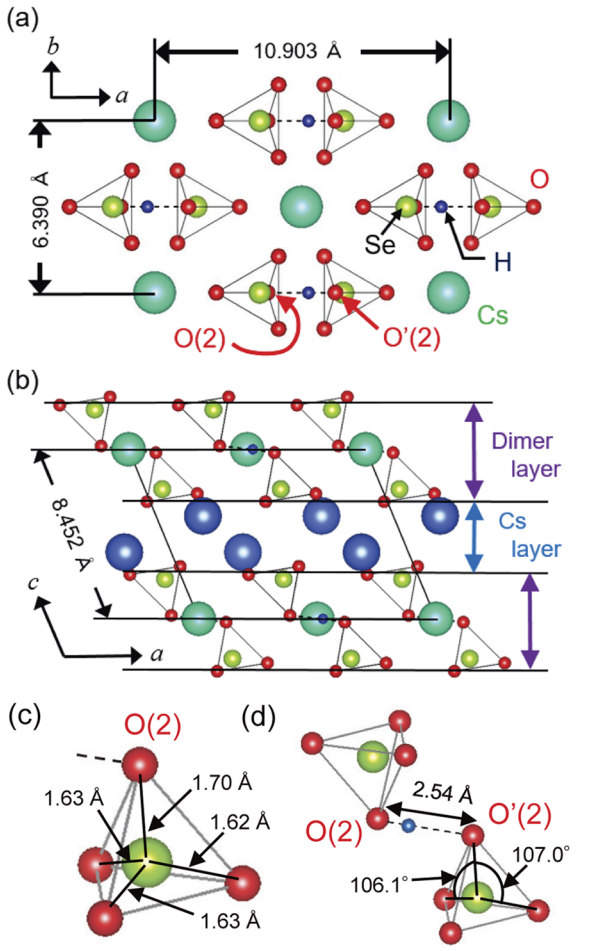

FIG. 1. Crystal structure of the *ab* (a) and *ac* planes (b) in phase III. Protons (blue small circles) are marked on the O(2)–O′(2) segment parallel to the *a* axis. In (b), the Cs^+ ions in the dimer and Cs layers are denoted by green and blue large circles, respectively. Structures of the selenate and dimer are shown in (c) and (d) together with the lengths and angles.

Phase IV below $T_{III\text{-}IV}$ is an antiferroelectric (AF) ordering state of the proton.[48] In the deuterated substance [$Cs_3D(SeO_4)_2$], the transition temperature amazingly increases to 168 K, while the transition mechanism is unsolved at present. In the KDP crystal with a remarkable isotope effect, the ferroelectric phase transition was studied in light of a proton tunneling, deformation of PO_4, etc.[44,45,49] Furthermore, the AF-ordering temperature in the present family strongly depends on the types of alkaline metallic ions, while the origin is not clear. $Rb_3H(SeO_4)_2$ exhibits no dielectric transition suggesting a quantum paraelectricity, though $Rb_3D(SeO_4)_2$ transits at 92 K.[50] $K_3H(SeO_4)_2$ and $K_3D(SeO_4)_2$ undergo the AF ordering at 20 K and 103 K, respectively.[51]

In this paper, we show the anharmonicity of the vibrational state and the mechanism of intrabond transfers in phases III and IV of $Cs_3H(SeO_4)_2$. In order to identify which phonon couples to the proton, we have systematically measured the wide-range of absorbance spectra at 5–8000 cm^{-1}. Anomalous absorption bands are discussed in combination with the protonic fluctuation obtained from the spin–lattice relaxation rate. Through those results, we have demonstrated that the intrabond transfer holds three types of mechanisms: thermal hopping and PAPTs associated with the tetrahedral deformation and libration.

II. EXPERIMENTAL

$Cs_3H(SeO_4)_2$ single crystals are grown by a conventional slow-evaporation method. By cutting the single crystal, we made the platy sample with the *ab* plane and thickness of about 1 mm. The sample was stuck on a silicon substrate (10 × 10 mm^2) with a super glue, and then we ground the sample. The minimum thickness, however, was about 80 μm because cracks were introduced. The single-crystal sample was used for the terahertz (THz, 5–100 cm^{-1}) and far-infrared (FIR, 100–700 cm^{-1}) measurements. In the mid-infrared (MID, 700–8000 cm^{-1}) frequency range, the absorption due to the OH stretching mode is too large to measure in the single crystal. The thin-polycrystal sample (30 μm thick and 1 mm in diameter) was also prepared with the $Cs_3H(SeO_4)_2$ saturated solution (5 μl), which was dropped on the silicon substrate and left at 30 °C for a couple of days.

Infrared spectra at 8–1400 cm^{-1} were measured above 300 K so far,[52] but the spectral analysis was not performed at all. To detect the wide range of absorbance spectra at 6–350 K, we used

three different spectrometers: terahertz time-domain spectrometer (RT-20000, Tochigi Nikon, Japan), microscopic FIR spectrometer facilitated in SPring-8 (beam line BL43IR), and FT-IR spectrometer (FT/IR 6100LT, JASCO, Japan) equipped with a Cassegrain microscope (IRT-5000, JASCO, Japan). For the THz spectroscopy, we set the aperture at 1.2 mm in diameter and the resolution was 1 cm^{-1}. Thanks to the high intensity of light in SPring-8, the FIR spectra were successfully measured with the resolution of 2 cm^{-1} despite the narrow aperture of about 200 μm in diameter. For the MIR experiment, the aperture was fixed to be 100 × 100 μm^2 and the resolution was 4 cm^{-1}. Optical cryostats [HELI-TRAN LT3-110 (Advanced Research Systems, USA), Microstat-He (Oxford, UK), and ST-300MS (Janis, USA)] are installed in those spectrometers to change the sample temperatures.

DFT calculations for phase III are carried out with a CASTEP (the Center for Computational Materials Science of IMR, Tohoku University) that is capable of treating a lattice system. We used a basis [6-31G(d,p) for H, O, Se, and LanL2DZ for Cs] and a functional (B3LYP). The calculated result well reproduces the wide range of absorbance spectra, while there appear several anomalous bands, as mentioned later.

By using a pulse spectrometer (Prot1002MR, Thamway, Japan), the NMR experiment is performed at 11.2 MHz with the powder specimen. The ^{1}H spin–lattice relaxation rate (T_1^{-1}) is determined from an intensity of the FID (Free Induction Decay) signal following the saturation comb pulse. In $Cs_3H(SeO_4)_2$, the natural abundance ratio of ^{77}Se is 7.6%, which is much lower than about 100% of ^{133}Cs. The distance between ^{1}H and ^{133}Cs nuclear spins (3.195 Å and 3.680 Å) is shorter than that between ^{1}H nuclear spins (6.390 Å). Therefore, T_1^{-1} is dominated by a dipole–dipole fluctuation between the nuclear spins of proton and Cs nucleus, as described below,

$$T_1^{-1} = \sum_n \gamma_I^2 \gamma_S^2 \hbar^2 S(S+1) \times \left(\frac{1}{12} F^{(0)} \frac{\tau}{1+(\omega_I-\omega_S)^2\tau^2} + \frac{3}{2} F^{(1)} \frac{\tau}{1+\omega_I^2\tau^2} + \frac{3}{4} F^{(2)} \frac{\tau}{1+(\omega_I+\omega_S)^2\tau^2} \right), \quad (1)$$

where

$$F^{(q)} = \frac{k_1 k_{\bar{1}}}{(k_1+k_{\bar{1}})} \left(f_1^q f_1^{q^*} - f_1^q f_{\bar{1}}^{q^*} - f_{\bar{1}}^q f_1^{q^*} + f_{\bar{1}}^q f_{\bar{1}}^{q^*} \right). \quad (2)$$

In Eq. (1), γ_I and γ_S are gyromagnetic ratios, and ω_I and ω_S are resonance frequencies, where I and S denote the spin quantum numbers of proton and Cs nucleus, respectively. The τ and n represent a residence time and the number of nuclei that contribute to the relaxation, respectively. In Eq. (2), f_j^q (j = 1, $\bar{1}$, q = 0, 1, 2) depends on the direction and position of the spins of proton and Cs nucleus and k_i is the transition rate between the two equivalent sites (i = 1 or $\bar{1}$).

III. RESULTS

A. Wide range of absorbance spectra

The absorbance spectra for the a and b polarizations [red and blue curves in Figs. 2(a) and 2(b)] are obtained with the single-crystal sample in THz and FIR ranges. The THz and MIR spectra for the filmy-polycrystal sample are shown by black curves in Figs. 2(a) and 2(c). Several phonon modes (ν_{pi}, i = 1–3) are observed in Fig. 2(a). The resonance frequency of ν_{pi} exhibits a hardening down to 6 K in Fig. 3(a). As shown in Fig. 3(b), the full width at half maximum (FWHM) of ν_{p1} and ν_{p3} (red and blue open squares) is reduced at low temperatures, though ν_{p2} (green solid squares) is anomalously broadened below 130 K and sharpened at 6 K.

The absorbance spectrum obtained by the DFT calculation is shown in Fig. 4(a) that almost agrees with Fig. 2. In the calculation, a OH stretching mode appears at 2380 cm^{-1}, the intensity of which is about ten times as large as one at around 900 cm^{-1}. In Fig. 4(b), the ν_{p2} phonon generates an asymmetric Cs^+ vibration in the ac plane. The SeO_4^{2-} tetrahedron slightly rotates, while the SeO_4H^- vibrates slightly. The slight rotation collectively modulates the O(2)–O′(2) distance.

In Fig. 2(a), the intensity overloads above 70 cm^{-1} in the single-crystal sample, suggesting the presence of large absorption. In the polycrystal sample, the anomalous band that has extremely broad width (~50 cm^{-1}) is well fitted with a Lorentzian curve at around 85 cm^{-1} (green curve at 6 K). The maximum shifts to lower the wavenumber by 5 cm^{-1} from 6 K to 300 K. This band is hardly assigned to conventional phonons or molecular vibrations.

In the FIR range [Fig. 2(b)], distinct absorption bands are observed at around 180 cm^{-1} and 400 cm^{-1}. The former band is identified as a librational mode of the dimer. As illustrated in Fig. 4(c), each SeO_4 tetrahedron is less distorted but collectively librates to the same direction. The libration leads to the most remarkable modulation of the O(2)–O′(2) distance among the phonons and molecular vibrations. The spectrum is highly deformed from a single Lorentzian curve at 50–60 K for the a polarization [Fig. 5(a)] and at 30–50 K for the b [Fig. 5(b)]. Those deformations are reproduced with two Lorentzian curves (red and blue curves), and thus the libration is found to split in connection with the AF ordering. Except for the libration, the spectrum in Fig. 2 alters slightly at around $T_{\text{III-IV}}$. Since the crystal symmetry is unchanged by the AF ordering, the libration makes a significant contribution to the transition mechanism of AF ordering.

Several absorption bands at 300–440 cm^{-1} in Fig. 2(b) are assigned to be a tetrahedral deformation of $(SeO_4)^{2-}$ and $(SeO_4H)^-$ generated by the O–Se–O bending without SeO stretching. The vibrational motif of the 440-cm^{-1} band (δ_{440}) is shown in Fig. 4(d). The deformation is accompanied by a modulation of the O(2)–O′(2) distance. In Fig. 3(b), the FWHM of δ_{440} takes anomalous maximum in the vicinity of 150 K at which no structural phase transition takes place.

In the calculated spectrum [Fig. 4(a)], a large absorption band appears at 660 cm^{-1}. In Fig. 2(c), however, such a band is actually observed above 700 cm^{-1}. A tiny absorption at 610 cm^{-1} indicated by arrows in Fig. 2(b) is different from a molecular vibration or conversion mode of the libration and δ_{440} because no spectral deformation is observed at 30–70 K.

Since the separation between the two equivalent sites (0.52 Å) is very short in comparison with LDS-1 (0.82 Å),[47] a conventional proton tunneling is possible to occur. A sharp absorption due to an optical transition between split levels may be observed, and the integrated absorbance should remarkably increase at low temperature. Such a band, however, is hardly found in Figs. 2(a) and 2(b), and

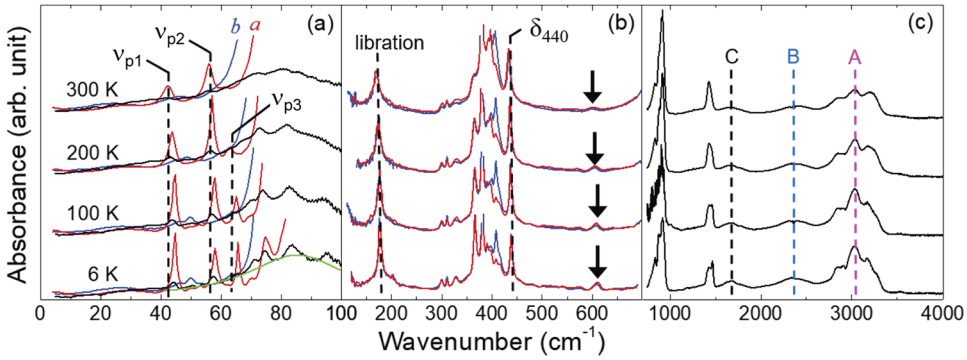

FIG. 2. Absorbance spectra in the ranges of THz (a), FIR (b), and MIR (c). In (a) and (b), red and blue curves for the single-crystal sample show the absorbance spectra polarized to the *a* and *b* axes, respectively. Black curves in (a) and (c) are obtained with the polycrystal sample. The broad band at around 85 cm^{-1} is well fitted with a Lorentzian curve that is shown at 6 K.

thus conventional proton tunneling is never generated in the present system.

In the MIR range [Fig. 2(c)], the large absorption at 700–1000 cm^{-1} comes from a tetrahedral deformation due to the SeO stretching without O–Se–O bending. The spectral shape changes slightly in phases III and IV. For example, the deformational motif at 880 cm^{-1} is illustrated in Fig. 4(e). The 1450-cm^{-1} band below 200 K is split into in-plane and out-of-plane OH bending modes with respect to the *ab* plane [Fig. 4(f)]. The broad absorption at 1000–2000 cm^{-1} (C band) arises from an overtone of the tetrahedral deformation. In the DFT calculation, no fundamental mode appears above 1500 cm^{-1} except for a OH stretching vibration at 2380 cm^{-1}. The characteristic broad bands at 2600–3300 (A band) and 2000–2600 cm^{-1} (B band) are related to the OH stretching vibration.

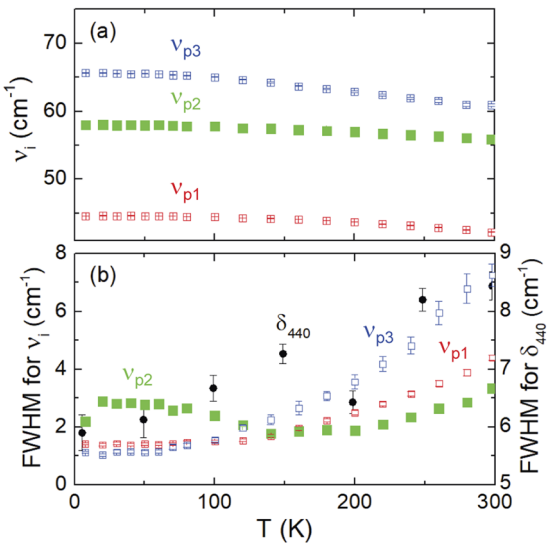

FIG. 3. Temperature dependence of the resonance frequencies for ν_{pi} (i = 1–3) (a). In (b), the full width at half maximum (FWHM) of ν_{pi} vs left vertical axis is plotted by the same colored squares in (a). Black circles represent the FWHM of the 440-cm^{-1} band (δ_{440}) vs right vertical axis.

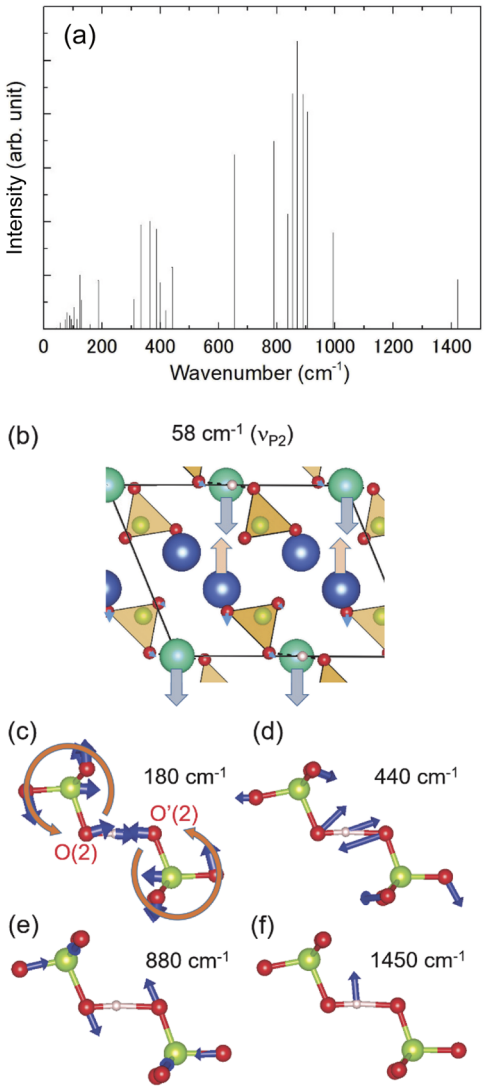

FIG. 4. Calculated spectrum below 1500 cm^{-1} (a) and vibrational motifs of 58-cm^{-1} (b), 180-cm^{-1} (c), 440-cm^{-1} (d), 880-cm^{-1} (e) and 1450-cm^{-1} (f) bands.

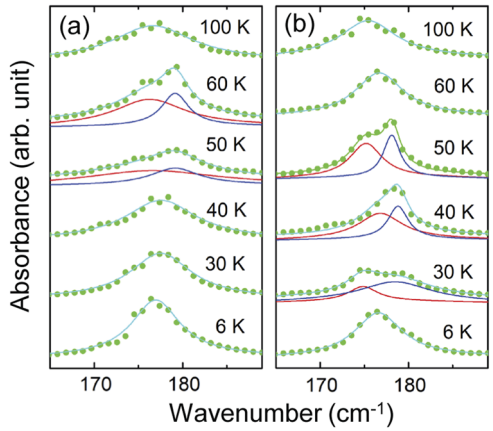

FIG. 5. Anomalous splittings of the libration in the vicinity of $T_{III\text{-}IV}$ along the *a* (a) and *b* (b) directions. The fitted results are shown by sky-blue curves.

B. Anharmonic-coupling calculations in the vibrational state

Characteristic broad absorption bands relevant to OH stretching vibrations are observed in many superprotonic conductors with MO_4^{2-} and in KDP families. For instance, three broad bands (so-called ABC bands) appear above 1000 cm^{-1} in $CsHSeO_4$.[53] Such bands were qualitatively inferred from an overtone, conversion mode, Fermi resonance, or anharmonic coupling to protons. Although the numerical calculations were attempted,[54] the quantitative explanation has not been succeeded yet. For the MIR spectrum, we have analyzed the vibrational potential to clarify the anharmonic coupling.

In general, anharmonic coupling of OH stretching mode to low-frequency vibration is important in a hydrogen-bonded system.[5,55] In gas-phase molecules such as carboxylic-acid and phosphinic-acid dimers with an intra-hydrogen bond, the broad OH stretching bands are simulated by considering a modulation of intradimer stretching.[56,57] In Fig. 2(c), the interval of fine peaks on the A band (~180 cm^{-1}) coincides with the librational frequency (ω_{lib}). This proves that the OH stretching vibration anharmonically couples to the libration. Although fine structures are hardly identified in the B band, the broad feature suggests an anharmonic coupling to a low frequency mode such as the libration or tetrahedral deformations. The B band is reproduced with a single Lorentzian curve (ω_B = 2350 cm^{-1} and FWHM = 275 cm^{-1}).

In order to reproduce the A-band shape, the anharmonic coupling of OH stretching vibration to the libration has been analyzed with a conventional method based on a parabolic potential and adiabatic approximation.[58] We consider an effective Hamiltonian ($H = H^0 + H^1$) for the ground state ($k = 0$) and the first excited one ($k = 1$) as follows:

$$H^0 = (a_{lib}^{+} a_{lib} + 1/2)\hbar\omega_{lib}, \tag{3}$$

$$H^1 = \left\{(a_{lib}^{+} a_{lib} + 1/2) + \lambda(a_{lib}^{+} + a_{lib}) - \lambda^2 + \omega_{OH}/\omega_{lib}\right\}\hbar\omega_{lib}. \tag{4}$$

Here, a_{lib}^{+} and a_{lib} are the creation and annihilation operators of the libration, respectively. The ω_{lib} and ω_{OH} denote the angular frequencies of libration and OH stretching vibration without anharmonic coupling, respectively. The off-diagonal term involves an anharmonic coupling constant λ. The eigenvalue at $k = 0$ is the same solution in a harmonic oscillator; $E_n^0 = (n + 1/2)\hbar\omega_{lib}$. Schrödinger equations are described with an eigenfrequency ($\omega_r^k = E_r^k/\hbar$) and an expansion coefficient ($C_{r,n}^k$). The wave function $|\Psi_r^1\rangle$ is expanded by the eigenfunction of libration ($|\Psi_n^0\rangle$) as a basis,

$$H^0 |\Psi_n^0\rangle = E_n^0 |\Psi_n^0\rangle, \tag{5}$$

$$H^1 |\Psi_r^1\rangle = E_r^1 |\Psi_r^1\rangle, \tag{6}$$

$$|\Psi_r^1\rangle = \sum_{n=1}^{N} C_{r,n}^1 |\Psi_n^0\rangle. \tag{7}$$

We set the number of basis functions at $N = 20$ in our FORTRAN program. The eigenfrequency ($\omega_r^1 = E_r^1/\hbar$) and expansion coefficient ($C_{r,n}^1$) are obtained by solving the eigenvalue problem for the 20 × 20 matrix.

A Fourier transform of the self-correlation function for the electric dipole moment provides a vibrational spectrum obeying a Lorentzian curve as follows:[5,58]

$$I(\omega) \propto \sum_{r,n} |C_{r,n}^1|^2 \exp\left(-\left(n + \frac{1}{2}\right)\frac{\hbar\omega_{lib}}{k_B T}\right) \times \frac{\Gamma}{\Gamma^2 + \left(\omega - \omega_r^1 + \left(n + \frac{1}{2}\right)\omega_{lib}\right)^2}, \tag{8}$$

where Γ^{-1} represents a life time of energy relaxation to the lattice system.

Figure 6 shows the least-squares fitted result on the basis of anharmonic-coupling calculation for the A band at 200–350 K (pink curves). The fitting parameters independent of temperature are determined as λ = 0.29 and ω_{OH} = 3050 cm^{-1}. The temperature dependence of the A band is dominated by Γ, as shown in Fig. 7. The higher the temperature, the larger the vibrational energy dissipates into the lattice system.

In Fig. 6, two fine bands on both sides of the central band at 3050 cm^{-1} have different intensities in comparison with nearly symmetric pink curves obtained by the calculation. To complete the fitting, an additional band (green Lorentzian curve) has to be introduced at 3200 cm^{-1}. The overtone of the OH bending band (1450 cm^{-1}) coincides with the A-band frequency. This implies that a Fermi resonance[58,59] splits the OH stretching vibration into 3050-cm^{-1} and 3200-cm^{-1} bands. The integrated-absorbance ratio of the former band (pink curves) to the latter (green curves) is estimated to be 9:1. As a consequence, the OH stretching vibration anharmonically couples to both the libration and OH bending modes.

In Eq. (8), the exponential term dependent on temperature represents the occupation rate of the first excited state of libration (180 cm^{-1} = 270 K). Since the excitation is highly reduced at low temperature, the fine structure should not appear but is observable down to 6 K. Through the anharmonic coupling, the libration may be indirectly generated by a MIR light exciting the OH stretching vibration. This implies that the adiabatic approximation is not applicable at low temperature, but above 200 K, as shown in Fig. 6.

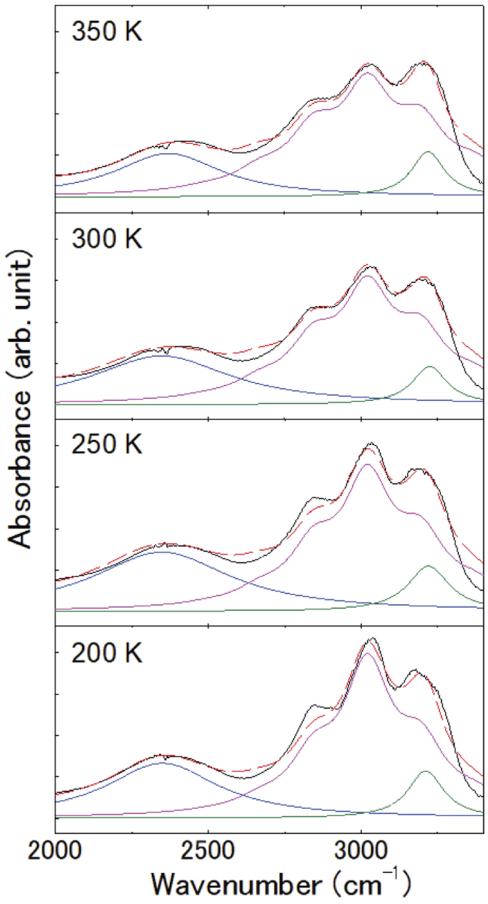

FIG. 6. Absorption spectra fitted with the anharmonic-coupling calculation at 200–350 K (black curve). The sum of three components (blue, green, and pink curves) is denoted by a red dashed curve.

C. Protonic potential of the vibrational state

The OH-stretching frequencies of the A and B bands have too large energy difference (700 cm^{-1}) to ascribe to symmetric or asymmetric vibrational modes. Those frequencies reflect the vibrational state of proton that is basically localized in either of the two equivalent sites of the dimer. In order to elucidate the vibrational state, we have analyzed the vibrational potential. A symmetric double well potential is not suitable for interpreting the present vibrational state so that we have solved the eigen-value problem for an asymmetric double minimum potential; $U(x) = ax^2 + bx^3 + cx^4$.[60] The eigenstate ($|\Psi_i\rangle$) is expanded by the eigenfunctions of $|u_n\rangle$ for a harmonic oscillator as a basis,

$$|\Psi_i\rangle = \sum_{n=0}^{N-1} C_{i,n}\,|u_n\rangle, \tag{9}$$

where $C_{i,n}$ and N denote an expansion coefficient and the number of basis functions, respectively. To obtain the eigenenergy for the i-th level (E_i) and $C_{i,n}$, we have diagonalized the matrix ($H_{m,n} = \langle u_m|H|u_n\rangle$) for $N = 50$.

The optimized potential is illustrated in Fig. 8, where the separation between two minima is 0.52 Å.[40] The energy difference in between $i = 1$ and 2 is equivalent to 700 cm^{-1}, and consequently, the A and B bands originate from the 0–2 and 0–1 transitions, respectively. The 0–1 transition probability is comparable to the 0–2 one, and those are one-order of magnitude higher than the 0–3 one.

We first consider the case that two kinds of parabolic potentials with different minimum energies are well separated, deep and shallow potentials. The first excited state for the deep potential is assumed to have identical energy to the ground state for the shallow one. Then, as those original potentials approach each other, asymmetric double-minimum potential is obtained similar to Fig. 8. If the wave functions for the original first excited state and ground one overlap, split levels emerge through a tunneling. In the present system, the excited levels of $i = 1$ and 2 stem from the tunneling in between those states. Since the wave functions have a single node at $-0.5 < x < 0$, those levels are strongly characterized by the original first excited state for the deep minimum. The anharmonic coupling calculation mentioned previously deals with a parabolic potential, which approximates the deep minimum side of the asymmetric double minimum potential. We should note that the deep minimum is on the left-hand side of the barrier in Fig. 8, though the crystal possesses equivalent amounts of the asymmetric potential with a deep minimum on the right-hand side.

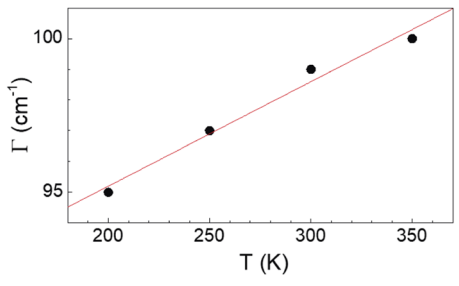

FIG. 7. Temperature dependence of Γ fitted with a red straight line.

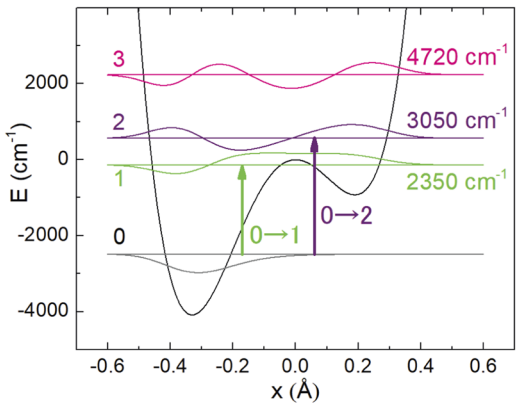

FIG. 8. Energy level scheme for the asymmetric double minimum potential in the vibrational state of proton. The wave functions are shown in each level (i = 0–3).

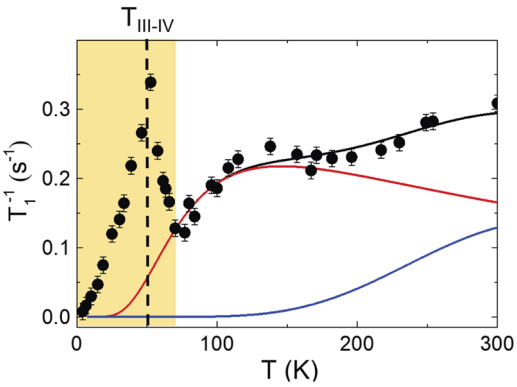

FIG. 9. Temperature dependence of the spin–lattice relaxation rate (black circles). A black curve is the sum of two different contributions (blue and red curves).

The anharmonic potential in Fig. 8 stands for the average vibrational nature of the localized proton that contributes to the O–H covalent bond. Above $T_{\text{III-IV}}$, the proton of every dimer is randomly distributed in either of the equivalent sites. There could be some mechanisms of intrabond transfers between those sites.

D. Protonic fluctuations in the dimer

The spin–lattice relaxation rate (T_1^{-1}) as a function of temperature has been measured to deduce the dynamical fluctuation that originates from the intrabond transfer. In Fig. 9, T_1^{-1} decreases down to 70 K by the way of a shallow maximum at around 150 K. The reduction from 300 K to 200 K is consistent with a conventional mechanism for insulators, while the maximum is hardly explained in the same way. In Fig. 3(b), δ_{440} takes anomalous maximum at 150 K as well. The coincidence suggests that the phonon contributes to the protonic fluctuation.

A residence time (τ) in Eq. (1) usually obeys an activation type as follows:[61]

$$\tau = \tau_0 \exp\left(-E^{\text{SL}}/k_{\text{B}}T\right), \tag{10}$$

where E^{SL} and τ_0 represent an energy barrier height and residence time, respectively. Above 70 K in Fig. 9, T_1^{-1} is fundamentally reproduced with two components as indicated by blue and red curves. The former component has E_1^{SL} = 76 meV (≈610 cm^{-1} ≈ 5.5 × 10^{-14} s), and the latter E_2^{SL} = 15.2 meV (≈123 cm^{-1} ≈ 183 K). The steep increase occurs below 70 K in agreement with the splitting temperature of the libration in Fig. 5. The protonic fluctuations are largely enhanced owing to a critical slowing down in connection with the AF ordering. The emergence of those fluctuations below 300 K reveals that the intrabond transfer possesses three different mechanisms.

IV. DISCUSSION

The magnitude of E_1^{SL} is comparable to an activation energy in usual proton conductors,[1,62] and the blue curve in Fig. 9 tends to increase above 150 K. Then, the first mechanism of intrabond transfer is attributed to a thermal hopping between the two equivalent sites. The hopping is qualitatively expressed with a symmetric double well potential as illustrated by a black curve in Fig. 10. The barrier height at x = 0 is approximated as E_1^{SL}. The two minima are shown in accordance with each ground state of the vibrational potentials, as mentioned above (red and blue dashed curves). In Fig. 2(b), the anomalous absorption is observed in the vicinity of 610 cm^{-1} that coincides with E_1^{SL}. This implies that a FIR light collectively excites the hopping motion. Since the 610-cm^{-1} band is almost independent of temperature below 300 K, we can regard the potential as rigid, and the hopping is little affected by the phonons and molecular vibrations. The shape of the potential is basically specified by the average O(2)–O′(2) distance.

From the fitting, the residence time of the first mechanism (τ_{01}) is evaluated to be 1.1 ns, indicating in the average time scale that the proton is localized in either of the two equivalent sites. On the other hand, the hopping motion is characterized as the time scale of 0.06 ps that is estimated from the resonance frequency (610 cm^{-1}). The proton localization is preserved with five orders of magnitude longer than the hopping motion. Owing to the extremely short duration of hopping and small transfer rate, the 610-cm^{-1} band may have very weak intensity compared to the libration and tetrahedral deformation. The time-averaging spectra in Fig. 2 are predominated by the vibrational state of the localized proton rather than the hopping transfer.

The second contribution of T_1^{-1} shows the anomalous maximum at around 150 K (red curve in Fig. 9). In addition, E_2^{SL} is too small to assign the second mechanism to a thermal hopping. Because the anharmonic coupling is significant in this system, as mentioned previously, we expect that the proton never transfers independently but correlates with the phonons or molecular vibrations. The FWHM of δ_{440} takes an anomalous maximum at 150 K [Fig. 3(b)] similar to the T_1^{-1}. Those results reveal that δ_{440} corresponds to the phonon correlating with the proton, and then a PAPT associated with the tetrahedral deformation [PAPT(def)] is considered to play an essential role in the second mechanism. In this case, the protonic motion obeys a time-varying double-minimum potential in contrast to the rigid one in the first mechanism. In other

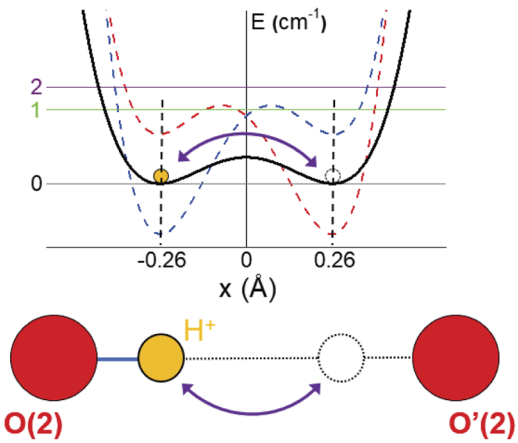

FIG. 10. Qualitative potential of the thermal hopping (black curve) together with the vibrational potentials (red and blue dashed curves). The separation between two minima is 0.52 Å.

words, the separation between the two minima changes from 0.52 Å. The wave functions of the ground state in each minimum dynamically overlap through the modulation of the O(2)–O′(2) distance generated by the δ_{440} phonon. As the O(2)–O′(2) distance shrinks, the separation between the two equivalent sites is shortened and, simultaneously, the barrier height is reduced.

Theoretical calculations on PAPT show that the residence time determined from NMR experiments is given by the identical relation to Eq. (10).[61] It should be noted here that E_2^{SL} represents a splitting energy between the ground state ($n = 0$) and the first excited one ($n = 1$). Those splitting levels are dynamically induced by the proton tunneling in the time-varying double minimum potential. The increment of red curve down to 150 K in Fig. 9 represents the enhancement of the 0–1 transition probability. The protonic fluctuation, however, diminishes below 150 K.[63] This indicates that the PAPT(def) is inhibited at low temperature because the thermal excitation of tetrahedral deformation is suppressed. The red curve in Fig. 9 is fitted with $\tau_{02} = 6.8$ ns, which is six times as long as τ_{01}. From the resonance frequency of δ_{440}, the time scale of the tunneling is comparable to ~ 0.08 ps that is much faster than τ_{02}.

We would like to emphasize that E_2^{SL} (= 123 cm^{-1}) is well consistent with the peak frequency (~ 85 cm^{-1}) of the anomalous broad band [Fig. 2(a)]. The consistency supports that the anomalous band corresponds to the optical transition between the splitting levels ($n = 0$ and 1). In usual proton tunneling as observed in LDS-1,[47] the 0–1 transition probability for a rigid double minimum potential increases at low temperature because an occupancy of the ground state increases. In contrast, the integrated absorbance of the 85-cm^{-1} band [Fig. 2(a)] varies slightly at 6–300 K. Dynamical proton conductivity due to an intrabond transfer was theoretically calculated by treating a PL interaction.[24] From the calculation, an absorption band is expected to appear in the THz frequency range below and above $T_{I\text{-}II}$. The characteristic behavior of the 85-cm^{-1} band is rationalized as a consequence of the PAPT(def). The 85-cm^{-1} band is observed even below $T_{III\text{-}IV}$ so that the PAPT(def) is collectively excited by the THz light, and the AF ordering may be broken (85 cm^{-1} = 127 K > $T_{III\text{-}IV}$).

The intrabond transfers due to the thermal hopping and PAPT(def) are suppressed below 70 K. The AF ordering is never conducted by those mechanisms, but by the third one. In Fig. 9, the fluctuation drastically develops from 70 K to $T_{III\text{-}IV}$. In the same temperature range, the libration along the a axis exhibits the anomalous splitting [Fig. 5(a)]. Below $T_{III\text{-}IV}$, the large fluctuation still remains and the libration along the b axis shows the splitting [Fig. 5(b)]. Those anomalies suggest that the PAPT relevant to the libration [PAPT(lib)] yields the third mechanism.

In gas-phase molecules with strong intrahydrogen bonds such as tropolone[64,65] and malonaldehydes,[66,67] the proton tunneling affects the entire molecular vibrations and rotations and all the absorption bands exhibit a splitting. As far as we know, such tunneling and splitting have not been observed in crystalline systems. Thanks to the strong hydrogen bond in the dimer, distinct splitting emerges in the libration. The PAPT(lib) helps the transfer and antiferroelectric arrangement of the proton. This is because the libration induces the most remarkable modulation of the O(2)–O′(2) distance among the vibrational modes. As the protonic fluctuation is enhanced toward the AF ordering, the rotational amplitude of each tetrahedron becomes large, and the drastic O(2)–O′(2) modulation may increase the tunneling probability between the two equivalent sites. The PAPT(lib) is considered to occur in the time scale of 0.2 ps that is evaluated from the vibrational period of libration. The characteristic time is four orders of magnitude faster than τ_{01} and τ_{02}.

Through the PL interaction, the proton also couples to ν_{p2}, which may not be a driving force of the AF ordering but sensitively responds to the protonic fluctuation. Figure 3(b) indicates that the fluctuation starts to appear at around 130 K below which the FWHM is broadened. By analogy with aforementioned gas-phase molecules, the broadening might reflect a splitting that is not clearly identified in the spectrum. Toward the AF ordering, a Coulomb interaction between the protons may develop in the crystal. The AF arrangement is completed at 6 K because the FWHM of ν_{p2} is sharpened [Fig. 3(b)], and the splitting of libration disappears (Fig. 5). Since T_1^{-1} approaches zero at 6 K (Fig. 9), the protonic fluctuation also diminishes.

Whenever the wave functions in both the equivalent sites overlap owing to the PAPT(def), the protonic ground state in the time-varying double minimum potential is considered to split into bonding state (+) and antibonding one (−). Through the PL interaction, the change of the protonic state mutually influences to the libration, each energy level of which may be split by analogy with the gas-phase molecules. The libration is described with an anharmonic Morse potential in which the ground state may be split into E_0^+ and E_0^- ($\Delta_0 = E_0^- - E_0^+$) and the first excited one into E_1^+ and E_1^- ($\Delta_1 = E_1^- - E_1^+$). In Fig. 5, the red and blue bands are probably related to the excitation of $E_0^- \rightarrow E_1^+$ and $E_0^+ \rightarrow E_1^-$, respectively. The difference of peak frequencies in those bands is obtained as 3 cm^{-1} that should be identical to $\Delta_0 + \Delta_1$. If we assume $\Delta_0 \sim \Delta_1$, the splitting energy for each level could be evaluated to be 1.5 cm^{-1} (~50 GHz), which is comparable to the value in tropolone (~0.9 cm^{-1}).[65] Therefore, the overlapping of wave functions is expected to be small in comparison with a conventional proton tunneling. Nevertheless, the dynamical proton tunneling at the narrowest O(2)–O′(2) distance is not selectively extracted in the present time-averaging spectrum. As the largest overlapping is achieved at the narrowest O(2)–O′(2) distance, the energy splitting may become larger than 1.5 cm^{-1}.

In Figs. 5(a) and 5(b), the splitting is observed in the different temperature ranges for the a and b polarizations. This reveals that the AF ordering established along a down to $T_{III\text{-}IV}$ is followed by the fluctuation generated along b. In Fig. 9(a), T_1^{-1} below $T_{III\text{-}IV}$ tends to decrease with a gradual slope compared to usual phase transitions. This tendency is consistent with the slight reduction in the dielectric constant down to 10 K.[48] Those results suggest that the AF arrangement also occurs along the b direction below $T_{III\text{-}IV}$.

V. CONCLUSIONS

Employing the single-crystal and thin-polycrystal samples of $Cs_3H(SeO_4)_2$, the wide range of absorbance spectra have been observed in phases III and IV, where the proton is basically localized in the dimer. The absorption bands are identified together with the DFT calculations, while there appear some anomalous bands (ν_{p2}, libration, tetrahedral deformation (δ_{440}), and 610-cm^{-1} band). The

OH stretching bands have extremely broad absorption at around 2350 cm^{-1} (B band) and 3050 cm^{-1} (A band). The B band is basically reproduced with a single Lorentzian curve. The A band possesses fine structures with the interval of 180 cm^{-1} in agreement with the resonance frequency of the libration. From the anharmonic-coupling calculation, the A band is found to couple not only to the libration but also to the OH bending mode. The A and B bands originate from the 0–2 and 0–1 transitions in the asymmetric double minimum potential, respectively, which expresses the vibrational state of the proton basically localized in either of the two equivalent sites.

The time-averaging spectra mainly reflect the vibrational state, while the proton is capable of transferring between the two equivalent sites even in the localized phase III. To elucidate the intrabond transfer between those sites, the protonic fluctuation is examined with T_1^{-1} in the ^{1}H-NMR experiment. Taking the anomalous bands into account, we have demonstrated that the intrabond transfer in the dimer possesses three different mechanisms. The intrabond transfer above 70 K is dominated by the thermal hopping and PAPT(def). The collective excitation relevant to the hopping is detected at around 610 cm^{-1} with weak intensity. The hopping motion is qualitatively described with a rigid symmetric double minimum potential that has the energy barrier of about 610 cm^{-1}. On the other hand, the PAPT(def) is the dynamical protonic motion in the time-varying symmetric double minimum potential. The distance between the minima is modulated through the tetrahedral deformation. The residence times estimated for those mechanisms indicate that the intrabond transfer (pico-second order) has extremely shorter duration than the vibrational state (nano-second order). Because of the quite different time scales, we are available to deal approximately with the intrabond transfer separately from the vibrational state.

The intrabond transfer below 70 K is attributed to the third mechanism, which is necessary to transport and arrange the proton antiferroelectrically. The splitting appears in the libration at 30–70 K. In the same temperature range, T_1^{-1} exhibits the huge enhancement because the fluctuation increases toward the AF ordering. Those results reveal that the PAPT(lib) becomes a driving force of the AF ordering. The protonic state is qualitatively described with a symmetric double minimum potential, where the distance between the minima (two equivalent sites) is dynamically modulated by the libration. As the wave functions overlap at the short distance, the tunneling occurs and the ground state is split into the bonding and anti-bonding bands. According to the PL interaction, the tunneling effect mutually influences the libration in which each energy level is also split. The splitting of the libration observed at 30–70 K arises from the optical transition between those split levels. Additionally, the protonic fluctuation is reflected in the ν_{p2} phonon, for which the FWHM exhibits anomalous broadening below 130 K, at which Coulomb interactions between the protons may start to develop toward the AF ordering.

Thanks to the systematic study, we have successfully confirmed the phonon in connection with the PAPT. At 300 K in Fig. 9, the PAPT(def) brings large fluctuation compared to the thermal hopping. From the extrapolation to $T_{I\text{-}II}$, we suspect that the thermal hopping makes a predominant contribution to the intrabond transfer, while the PAPT(def) still contributes. We should carefully investigate such quantum-mechanical effects even at high temperature. An interbond transfer is expected to play a significant role in addition to the intrabond one in the superprotonic phase. The wide range of absorption spectra and protonic fluctuations in phases I and II are the next research subjects to identify which phonons or molecular vibrations contribute not only to the interbond transfer but also to the precursory phenomenon.

ACKNOWLEDGMENTS

This work was supported by the JSPS KAKENHI (Grant Nos. 24340071, 24651127, 15H03851, and 17K05825). The synchrotron radiation experiments were performed at the BL43IR of SPring-8 with the approval of JASRI (Proposal Nos. 2015A1418, 2016A1337, 2016B1321, 2017B1149, and 2019A1081). The authors acknowledge the Center for Computational Materials Science of IMR, Tohoku University (Grant Nos. 19S0203 and 18S0206). We would like to thank Professor H. Matsumoto, Professor M. Takahashi, S. Takano, S. Miyoshi, and A. Tomida for fruitful discussions. We would also like to thank Professor S. Ikehata and his students for the measurement and discussion of the NMR experiment.

REFERENCES

[1] P. Colomban, *Proton Conductors* (Cambridge University, Cambridge, 1992).
[2] K.-D. Kreuer, Chem. Mater. **8**, 610 (1996).
[3] H. Sirringhaus, Adv. Mater. **21**, 3859 (2009).
[4] T. Norby, Nature **410**, 877 (2001).
[5] Y. Marechal, *The Hydrogen Bond and the Water Molecule* (Elsevier, Amsterdam, 2007).
[6] G. Gilli and P. Gilli, *The Nature of the Hydrogen Bond* (Oxford University, Oxford, 2009).
[7] K.-D. Kreuer, S. J. Paddison, E. Spohr, and M. Schuster, Chem. Rev. **104**, 4637 (2004).
[8] Y. Maniwa, K. Matsuda, H. Kyakuno, S. Ogasawara, T. Hibi, H. Kadowaki, S. Suzuki, Y. Achiba, and H. Kataura, Nat. Mater. **6**, 135 (2007).
[9] H. Matsui, Y. Ohhta, C. Iida, M. Horii, and M. Tadokoro, J. Phys. Soc. Jpn. **79**, 103601 (2010).
[10] H. Matsui and M. Tadokoro, J. Chem. Phys. **137**, 144503 (2012).
[11] H. Matsui, Y. Suzuki, H. Fukumochi, and M. Tadokoro, J. Phys. Soc. Jpn. **83**, 054708 (2014).
[12] H. Matsui, T. Sasaki, and M. Tadokoro, J. Phys. Chem. C **123**, 20413 (2019).
[13] Y. Matsuo, H. Ikeda, T. Kawabata, J. Hatori, and H. Oyama, Mat. Sci. Appl. **08**, 747 (2017).
[14] M. I. Vladu, P. A. Troshin, M. Reisinger, L. Shmygleva, Y. Kanbur, G. Schwabegger, M. Bodea, R. Schwödiauer, A. Mumyatov, J. W. Fergus, V. F. Razumov, H. Sitter, N. S. Sariciftci, and S. Bauer, Adv. Funct. Mater. **20**, 4069 (2010).
[15] C. Zhong, Y. Deng, A. F. Roudsari, A. Kapetanovic, M. P. Anantram, and M. Rolandi, Nat. Commun. **2**, 476 (2011).
[16] T. Miyake, E. E. Josberger, S. Keene, Y. Deng, and M. Rolandi, APL Mater. **3**, 014906 (2015).
[17] E. E. Josberger, P. Hassanzadeh, Y. Deng, J. Sohn, M. J. Rego, C. T. Amemiya, and M. Rolandi, Sci. Adv. **2**, e1600112 (2016).
[18] P. Feng, P. Du, C. Wan, Y. Shi, and Q. Wan, Sci. Rep. **6**, 34065 (2016).
[19] S. M. Haile, D. A. Boysen, C. R. I. Chisholm, and R. B. Merle, Nature **410**, 910 (2001).
[20] K. D. Kreuer, Annu. Rev. Mater. Res. **33**, 333 (2003).
[21] Y. Zhou, X. Guan, H. Zhou, K. Ramadoss, S. Adam, H. Liu, S. Lee, J. Shi, M. Tsuchiya, D. D. Fong, and S. Ramanathan, Nature **534**, 231 (2016).
[22] N. I. Pavlenko, J. Chem. Phys. **112**, 8637 (2000).
[23] N. I. Pavlenko, Phys. Rev. B **61**, 4988 (2000).

[24]N. I. Pavlenko and I. V. Stasyuk, J. Chem. Phys. **114**, 4607 (2001).
[25]D. Merunka and B. Rakvin, Phys. Rev. B **79**, 132108 (2009).
[26]J. Dolinsek, U. Mikac, J. E. Javorsek, G. Lahajnar, and R. Blinc, Phys. Rev. B **58**, 8445 (1998).
[27]J. Lasave, P. Abufager, and S. Koval, Phys. Rev. B **93**, 134112 (2016).
[28]D. Homouz, G. Reiter, J. Eckert, J. Mayers, and R. Blinc, Phys. Rev. Lett. **98**, 115502 (2007).
[29]G. Beutier, S. P. Collins, G. Nisbet, K. A. Akimova, E. N. Ovchinnikova, A. P. Oreshko, and V. E. Dmitrienko, Phys. Rev. B **92**, 214116 (2015).
[30]N. I. Pavlenko, A. Pietraszko, A. Pawlowski, M. Polomska, I. V. Stasyuk, and B. Hilczer, Phys. Rev. B **84**, 064303 (2011).
[31]F. Shikanai, K. Tomiyasu, N. Aso, S. Ikeda, and T. Kamiyama, Phys. Rev. B **80**, 144103 (2009).
[32]B. V. Merinov, A. I. Baranov, and L. A. Shuvalov, Sov. Phys. Crystallogr. **35**, 200 (1990).
[33]M. Ichikawa, T. Gustafsson, and I. Olovsson, Solid State Commun. **87**, 349 (1993).
[34]M. Komukae, K. Sakata, T. Osaka, and Y. Makita, J. Phys. Soc. Jpn. **63**, 1009 (1994).
[35]Y. Luspin, D. De Sousa Meneses, P. Simon, and G. Hauret, Eur. Phys. J. **10**, 215 (1999).
[36]Y. Matsuo, Y. Tanaka, J. Hatori, and S. Ikehata, Solid State Commun. **134**, 361 (2005).
[37]J. Hatori, Y. Matsuo, and S. Ikehata, Solid State Commun. **140**, 452 (2006).
[38]Y. Yoshida, J. Hatori, H. Kawakami, Y. Matsuo, and S. Ikehata, Symmetry **4**, 507 (2012).
[39]B. V. Merinov, N. B. Bolotina, A. I. Baranov, and L. A. Shuvalov, Sov. Phys. Crystallogr. **33**, 824 (1988).
[40]R. Sonntag, R. Melzer, T. Wessels, and P. G. Radaelli, Acta Cryst. C **53**, 1529 (1997).
[41]N. I. Pavlenko, J. Phys. Condens. Matter **11**, 5099 (1999).
[42]H. Kamimura, Solid State Ionics **180**, 471 (2009).
[43]T. Ito and H. Kamimura, J. Phys. Soc. Jpn. **67**, 1999 (1998).
[44]Y. Yamada and S. Ikeda, J. Phys. Soc. Jpn. **63**, 3691 (1994).
[45]S. Ikeda and Y. Yamada, Physica B **213-214**, 652 (1995).
[46]E. J. Supahr, L. Wen, M. Stavola, L. A. Boatner, L. C. Feldman, N. H. Tolk, and G. Lüpke, Phys. Rev. Lett. **102**, 075506 (2009).
[47]H. Matsui, K. Iwamoto, D. Mochizuki, S. Osada, Y. Asakura, and K. Kuroda, J. Chem. Phys. **143**, 024503 (2015).
[48]M. Komukae, T. Osaka, T. Kaneko, and Y. Makita, J. Phys. Soc. Jpn. **54**, 3401 (1985).
[49]G. Reiter, J. Mayers, and P. Platzman, Phys. Rev. Lett. **89**, 135505 (2002).
[50]K. Gesi, J. Phys. Soc. Jpn. **50**, 3185 (1981).
[51]M. Endo, T. Kaneko, T. Osaka, and Y. Makita, J. Phys. Soc. Jpn. **52**, 3829 (1983).
[52]V. Zelezný, J. Petzelt, Y. G. Goncharov, G. V. Kozlov, A. A. Volkov, and A. Pawlowski, Solid State Ionics **36**, 175 (1989).
[53]P. Colomban, M. Pham-thi, and A. Novak, J. Mol. Struct. **161**, 1 (1987).
[54]F. Fillaux, B. Marchon, and A. Novak, Chem. Phys. **86**, 127 (1984).
[55]Y. Marechal and A. Witkowski, J. Chem. Phys. **48**, 3697 (1968).
[56]P. Blaise, M. J. Wojcik, and O. Henri-Rousseau, J. Chem. Phys. **122**, 064306 (2005).
[57]N. Rekik, H. Ghalla, and G. Hanna, J. Phys. Chem. A **116**, 4495 (2012).
[58]O. H. Rousseau and P. Blaise, *Quantum Oscillators* (John Wiley & Sons, New Jersey, 2011).
[59]S. Ikeda, H. Sugimoto, and Y. Yamada, Phys. Rev. Lett. **81**, 5449 (1998).
[60]H. Matsumoto, T. Mori, K. Iwamoto, S. Goshima, S. Kushibiki, and N. Toyota, Phys. Rev. B **79**, 214306 (2009).
[61]J. L. Skinner and H. P. Trommsdorff, J. Chem. Phys. **89**, 897 (1988).
[62]X. Ke and I. Tanaka, Phys. Rev. B **69**, 165114 (2004).
[63]U. Mikac, B. Zalar, J. Dolinšek, J. Seliger, V. Žagar, O. Plyushch, and R. Blinc, Phys. Rev. B **61**, 197 (2000).
[64]R. L. Redington, T. E. Redington, and R. L. Sams, J. Phys. Chem. A **110**, 9633 (2006).
[65]K. Tanaka, H. Honjo, T. Tanaka, H. Kohguchi, Y. Ohshima, and Y. Endo, J. Chem. Phys. **110**, 1969 (1999).
[66]A. A. Arias, T. A. W. Wasserman, and P. H. Vaccaro, J. Chem. Phys. **107**, 5617 (1997).
[67]T. Baba, T. Tanaka, I. Morino, K. M. T. Yamada, and K. Tanaka, J. Chem. Phys. **110**, 4131 (1999).